Society of Medical Education & Research

2022, Volume 2, Issue 2, Page No: 125-141
ISSN: 3108-4834

Archive of International Journal of Cancer and Allied Science

Enhanced Cancer Nanovaccine Targeting the CXCL12/CXCR4 Axis Bidirectionally to Prevent Recurrence and Metastasis in Triple-Negative Breast Cancer

Rebecca Anne Wilson[1]*, Jennifer Sarah Miller[1]

[1]Department of Cancer Research, Stanford University School of Medicine, Palo Alto, United States.

***E-mail** ✉ r.wilson.stanford@gmail.com

Abstract

In situ cancer vaccines represent an emerging strategy in cancer immunotherapy; however, the local immunosuppressive microenvironment within tumors limits their immune activation and therapeutic efficacy. The CXCL12/CXCR4 axis is a critical mediator of this immunosuppressive environment. In this study, siCXCR4 (S) was employed as an "immune adjuvant" and co-delivered with hydroxycamptothecin (HCPT) to construct an in situ cancer nanovaccine (HCPT/S@CaP/HA) aimed at synergistically inhibiting the growth, recurrence, and metastasis of triple-negative breast cancer (TNBC). HCPT/S@CaP/HA actively targeted orthotopic TNBC cells and cancer-associated fibroblasts (CAFs), inducing immunogenic cell death of TNBC cells and promoting dendritic cell (DC) maturation. Concurrently, HCPT/S@CaP/HA reduced CXCL12 secretion by CAFs and silenced CXCR4 expression in TNBC tissues, thereby bidirectionally blocking the CXCL12/CXCR4 axis. This dual action synergistically reversed the immunosuppressive microenvironment, enhanced infiltration and activity of cytotoxic T lymphocytes in TNBC tissues, and inhibited tumor growth. Furthermore, HCPT/S@CaP/HA prevented TNBC recurrence by increasing memory T lymphocyte populations in mouse spleen tissue and suppressed spontaneous lung metastasis by enhancing tumor antigen presentation and activating TNBC-specific immune responses. Overall, HCPT/S@CaP/HA shows potential as an effective in situ nanovaccine for TNBC immunotherapy.

Keywords: Nanovaccine, CXCL12/CXCR4 axis, Breast cancer, Metastasis

Introduction

Triple-negative breast cancer (TNBC) is a highly heterogeneous subtype of breast cancer, characterized by the absence of estrogen receptor, progesterone receptor, and human epidermal growth factor receptor 2 expression. TNBC is the most aggressive and invasive form of breast cancer, predominantly affecting young women, with a propensity for early metastasis, high recurrence rates, and poor prognosis [1]. Although TNBC accounts for approximately 20% of breast cancer cases, it contributes to 83% of breast cancer-related mortality, making it the deadliest subtype [2].

Access this article online https://smerpub.com/

Received: 01 September 2022; **Accepted:** 27 November 2022

How to cite this article: Wilson RA, Miller JS. Enhanced Cancer Nanovaccine Targeting the CXCL12/CXCR4 Axis Bidirectionally to Prevent Recurrence and Metastasis in Triple-Negative Breast Cancer. Arch Int J Cancer Allied Sci. 2022;2(2):125-41. https://doi.org/10.51847/s9PU4WZ8wD

Recently, cancer immunotherapy has offered new therapeutic avenues for TNBC by enhancing patients' own immune responses, which are rapid and generally well-tolerated [3]. Immune checkpoint inhibitors targeting programmed death-1/programmed cell death ligand 1 (PD-1/PD-L1) have been FDA-approved for TNBC treatment, restoring cytotoxic T lymphocyte (CTL) activity against tumor cells [4]. However, only 10–30% of patients respond clinically, a phenomenon associated not only with individual variability in PD-L1 expression but also with the immunosuppressive tumor microenvironment of TNBC [5–8].

In situ cancer vaccines leverage patients' own tumor cells as antigens to elicit cancer-specific immune responses, providing a personalized immunotherapy strategy. Yet, conventional in situ vaccines often fail to trigger sufficient antigen release, and dendritic cells (DCs) exhibit limited capacity to process tumor antigens, resulting in suboptimal antigen-specific T cell responses. Moreover, effector T cells infiltrating tumor tissue may

become exhausted due to the immunosuppressive microenvironment, preventing effective tumor cell killing [9–12]. Theoretically, inducing immunogenic cell death (ICD) in tumor cells, promoting DC maturation, and reversing immunosuppression could enhance the efficacy of in situ vaccines.

Chemokine receptor CXCR4, a G-protein-coupled receptor with seven transmembrane domains, is highly expressed in TNBC compared with other breast cancer subtypes [13]. Its specific ligand, CXCL12, is primarily secreted by cancer-associated fibroblasts (CAFs) in solid tumors. Overexpression of CXCR4 or CXCL12 hypersecretion activates the CXCL12/CXCR4 axis, recruiting myeloid-derived suppressor cells (MDSCs) and regulatory T cells, inhibiting CTL activity, and promoting immune evasion [14–17]. Additionally, CXCL12 drives polarization of tumor-associated macrophages (TAMs) toward the M2 phenotype, further activating CAFs and establishing an immunosuppressive feedback loop [18]. This axis also mediates crosstalk between primary tumors and distant metastatic sites, for instance, between CXCL12-rich lung tissue and CXCR4-overexpressing TNBC cells [19]. Its activation is a key factor underlying the low response rate to PD-1/PD-L1 therapy in clinical settings [20] and facilitates epithelial–mesenchymal transition (EMT), enhancing TNBC invasiveness [21–24]. Thus, targeting the CXCL12/CXCR4 axis with siCXCR4 may reverse immunosuppression and inhibit TNBC metastasis.

Hydroxycamptothecin (HCPT) is a cytotoxic agent that induces apoptosis through DNA fragmentation and can trigger ICD, promoting tumor antigen release [25, 26]. Co-delivery of HCPT and siCXCR4 to TNBC tissues is expected to create a synergistic in situ cancer vaccine. However, HCPT's poor solubility in lipids and water [27, 28], along with the instability and negative charge of naked siCXCR4 [29–32], limits delivery efficiency. Here, calcium phosphate nanoparticles (CaP) were employed as carriers, facilitating complexation of Ca^{2+} with lactone ring-opened HCPT and hyaluronic acid (HA), and electrostatic adsorption with siCXCR4. This approach enabled efficient co-loading of HCPT and siCXCR4 via co-precipitation, yielding the in situ nanovaccine HCPT/S@CaP/HA. The nanovaccine accumulated in orthotopic TNBC tissues, activated adaptive immune responses, reversed immunosuppression in tumor, spleen, and lung tissues, and inhibited TNBC growth, recurrence, and metastasis **(Figure 1)**.

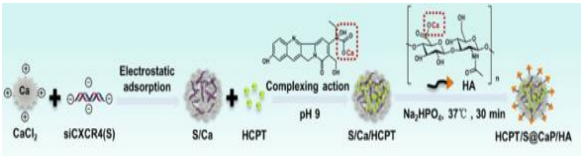

a)

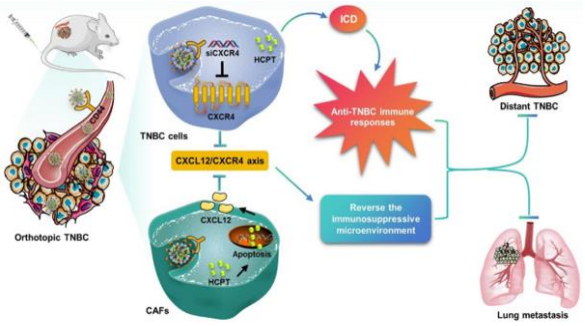

b)

Figure 1. Schematic representation of the synthesis and antitumor effects of HCPT/S@CaP/HA in a TNBC mouse model. (a) Process for preparing HCPT/S@CaP/HA. (b) Proposed mechanism of HCPT/S@CaP/HA-mediated TNBC therapy.

Results and Discussion

CXCL12/CXCR4 signaling drives 4T1 cell proliferation, migration, and invasion

Cancer-associated fibroblasts (CAFs) constitute a major fraction of the tumor stroma and actively regulate key aspects of tumor progression, including extracellular matrix deposition, tumor growth, metastatic potential, angiogenesis, and immunosuppression. Within the tumor microenvironment, CAFs are the predominant source of CXCL12, which engages CXCR4 on tumor cells to trigger downstream cascades such as PI3K, PLC, JAK/STAT, and MAPK pathways, influencing calcium signaling, adhesion, motility, stem cell recruitment, and the establishment of an immunosuppressive niche [33, 34].

Immunofluorescence analysis confirmed abundant CAF presence in orthotopic TNBC tissues, as evidenced by strong α-SMA and FAP1 signals **(Figure 2a)**. Exposure of NIH-3T3 fibroblasts to 4T1 cell-conditioned medium (4T1-CM) induced a significant upregulation of α-SMA, FAP1, and PDGFRβ, indicating phenotypic conversion into CAF-like cells **(Figures 2b–2d)** [35, 36]. While CXCR4 expression was pronounced in 4T1 cells, it remained minimal in both NIH-3T3 cells and derived CAFs. Conversely, CAFs secreted substantially more

CXCL12 than NIH-3T3 cells **(Figure 2e)**, demonstrating the functional activation of the CXCL12/CXCR4 axis between CAFs and TNBC cells in situ.

Functional assays revealed that NIH-3T3-conditioned medium had negligible impact on 4T1 proliferation, whereas CAF-conditioned medium significantly enhanced cell growth. Neutralization of CXCL12 markedly reduced this proliferative effect, highlighting the critical role of CAF-derived CXCL12 in driving tumor cell expansion **(Figure 2f)**. In addition, co-culture with CAFs substantially increased 4T1 cell migration and invasion. Interruption of the axis via CXCR4 blockade on 4T1 cells or CXCL12 neutralization in the transwell recipient chamber effectively suppressed these behaviors **(Figure 2g)**.

These data collectively indicate that CAF-secreted CXCL12 and tumor cell CXCR4 overexpression cooperate to activate the CXCL12/CXCR4 signaling axis, thereby enhancing TNBC cell proliferation, motility, and invasive capacity.

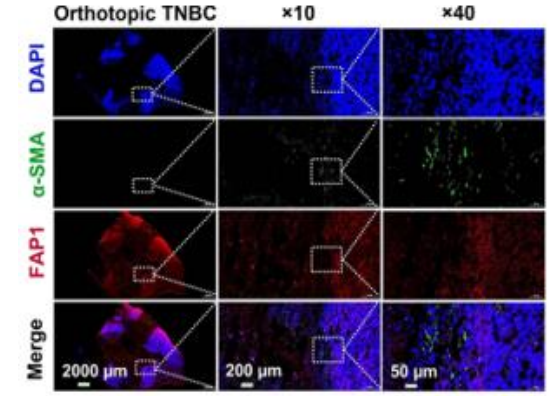

a)

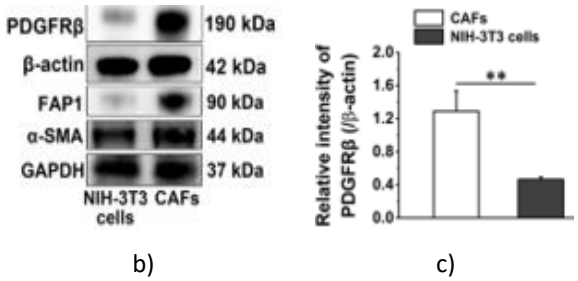

b) c)

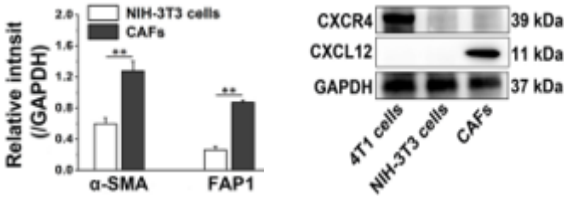

d) e)

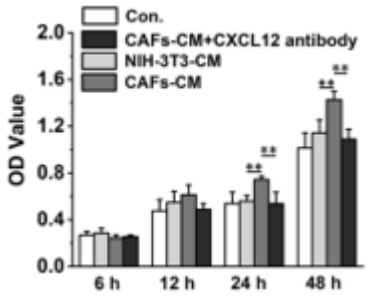

f)

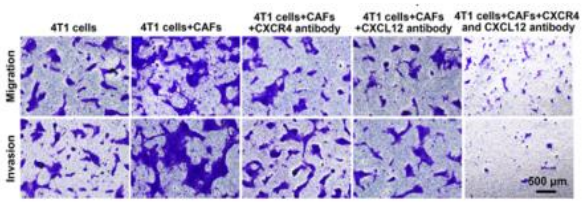

g)

Figure 2. CAF-Derived CXCL12 Promotes 4T1 Cell Proliferation, Migration, and Invasion. (a) Representative immunofluorescence images showing α-SMA and FAP1 expression in orthotopic TNBC tissues. (b–d) Comparative expression levels of α-SMA, FAP1, and PDGFRβ in NIH-3T3 cells and CAFs (n = 3). (e) CXCR4 and CXCL12 expression in 4T1 cells, NIH-3T3 cells, and CAFs. (f) Effects of CAF- and NIH-3T3-conditioned media on 4T1 cell proliferation (n = 6). (g) Impact of CAFs on 4T1 migration and invasion (n = 3). Data are presented as mean ± SD. **P < 0.01. Statistical significance was assessed using unpaired two-tailed Student's t-test (c–d) or one-way ANOVA with Tukey's post-hoc test (f).

Preparation and characterization of HCPT/S@CaP/HA

Calcium phosphate (CaP) nanoparticles are widely recognized as efficient carriers for small interfering RNA due to their high transfection efficiency, biocompatibility, and biodegradability [37]. HCPT contains a lactone ring that, under alkaline conditions, opens to expose carboxyl groups capable of binding Ca^{2+}. This property enables the incorporation of lactone ring-opened HCPT into the CaP core via complexation. Upon acidification in lysosomes, the HCPT reverts to its lactone form, which exhibits potent anticancer activity. In this study, CaP was employed to co-deliver HCPT and siCXCR4.

However, bare CaP tends to aggregate and shows poor stability, necessitating the use of a stabilizer. Hyaluronic acid (HA), a naturally occurring anionic polysaccharide rich in carboxyl groups, was used to stabilize the nanoparticles by binding Ca^{2+}, thereby improving particle stability **(Figure 3a)**.

Agarose gel electrophoresis confirmed that siCXCR4 was fully encapsulated within CaP at a Ca/P ratio of 12.5 **(Figure 3b)**. Thermogravimetric analysis (TGA) verified the presence of HCPT, CaP, and HA in the final HCPT/S@CaP/HA formulation. Dynamic light scattering showed that HCPT/S@CaP/HA had an average particle size of approximately 268 nm and a zeta potential of −20.4 mV **(Figure 3c)**. Importantly, particle size, polydispersity index (PDI), and HCPT content remained stable in PBS over 6 days **(Figure 3d)**.

When exposed to 10% FBS, naked siCXCR4 degraded substantially within 8 hours, whereas HCPT/S@CaP/HA effectively protected siCXCR4 for at least 24 hours **(Figure 3e)**. Release studies demonstrated that both HCPT and siCXCR4 were released more efficiently under acidic conditions **(Figures 3f and 3g)**. After 4 hours of incubation at pH 5.0, needle-like HCPT crystals were observed **(Figure 3h)**, similar to the crystallization pattern of lactone-type HCPT under the same conditions. This indicates that the lactone ring-opened HCPT released from the nanoparticles converts to the poorly soluble lactone form in acidic environments, forming crystals.

Finally, western blot analysis confirmed the gene silencing capability of HCPT/S@CaP/HA, showing comparable CXCR4 inhibition in 4T1 cells to the positive control siCXCR4@Lipofectamine 2000.

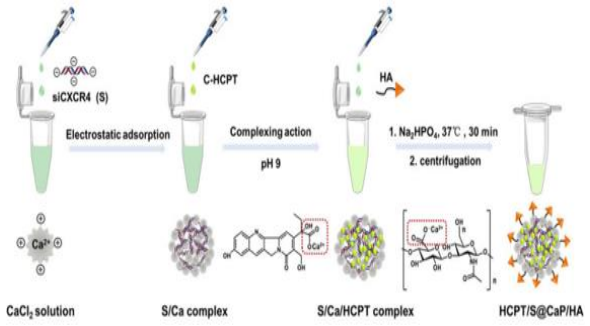

a)

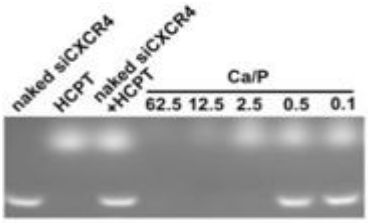

b)

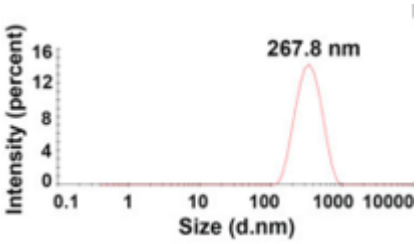

c)

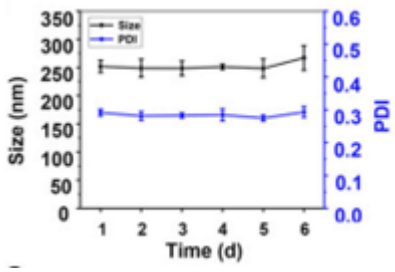

d)

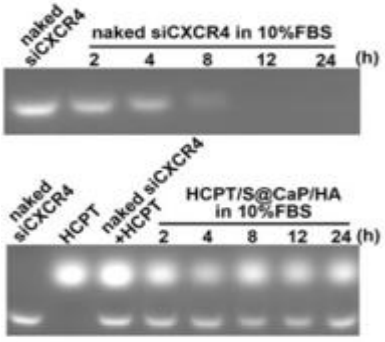

e)

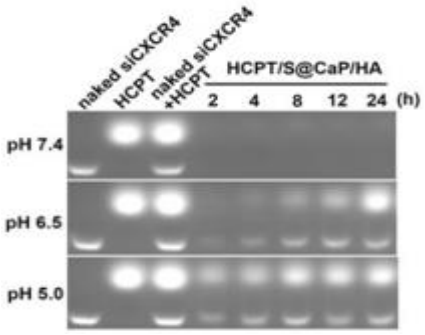

f)

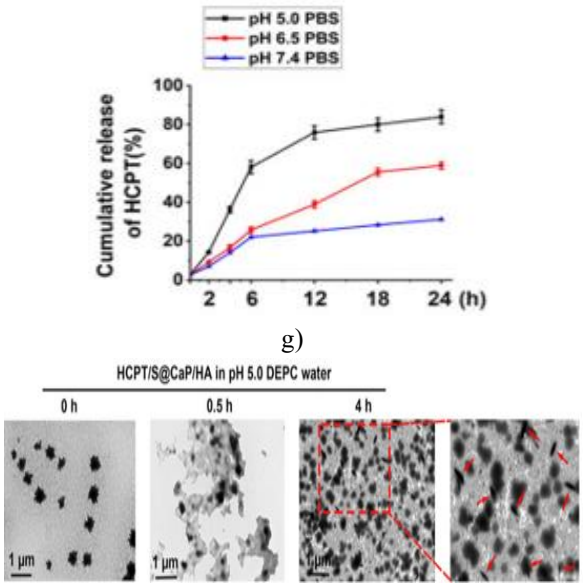

Figure 3. Characterization of HCPT/S@CaP/HA. (a) Schematic of HCPT/S@CaP/HA preparation. (b) Agarose gel electrophoresis showing siCXCR4 loading at different Ca/P ratios. (c) Particle size distribution of HCPT/S@CaP/HA. (d) Stability of HCPT/S@CaP/HA in PBS (pH 7.4). (e) Serum stability of siCXCR4. (f) pH-dependent release of siCXCR4 from HCPT/S@CaP/HA. (g) pH-dependent release of HCPT. (h) TEM images of HCPT/S@CaP/HA after incubation in pH 5.0 DEPC water. Data are presented as mean ± SD, n = 3.

HCPT/S@CaP/HA uptake by 4T1 cells and CAFs via CD44

CD44 functions as a cell surface receptor that specifically binds HA and mediates its internalization. By incorporating HA onto nanoparticles, cellular uptake can be enhanced. Immunofluorescence analysis revealed strong CD44 expression in 4T1 cells, as well as detectable expression in NIH-3T3 cells and CAFs. Following incubation with HCPT/cy5-S@CaP/HA, fluorescence intensity in both 4T1 cells and CAFs increased over time, indicating efficient nanoparticle internalization. Pre-treatment with free HA significantly reduced nanoparticle uptake in both cell types. Furthermore, NIH-3T3 cells internalized far less HCPT/cy5-S@CaP/HA than CAFs, and MDA-MB-453 cells, which express minimal CD44, exhibited significantly lower nanoparticle uptake compared with 4T1 cells. These results confirm that CD44-mediated endocytosis is the primary mechanism by which HCPT/S@CaP/HA enters 4T1 cells and CAFs.

Inhibition of 4T1 cell and CAF growth by HCPT/S@CaP/HA

Treatment with HCPT/S@CaP/HA markedly reduced 4T1 cell viability, live/dead cell ratio, and colony formation. CAF survival was similarly decreased following treatment. Western blot analysis revealed upregulation of pro-apoptotic Bax and cleaved caspase-3 and downregulation of anti-apoptotic Bcl-2 in both 4T1 cells and CAFs. Collectively, these results indicate that HCPT/S@CaP/HA effectively suppresses TNBC cell and CAF growth by activating the mitochondrial apoptotic pathway.

Bidirectional inhibition of 4T1 cell migration and invasion via CXCL12/CXCR4 axis blockade

Overexpression of CXCR4 triggers the CXCL12/CXCR4 axis, promoting epithelial–mesenchymal transition (EMT) in 4T1 cells and conferring migratory and invasive capabilities. Elevated MMP-9 levels further facilitate extracellular matrix degradation, enabling tumor cell detachment and metastasis [38]. Both S@CaP/HA and HCPT/S@CaP/HA effectively silenced CXCR4 expression in 4T1 cells **(Figure 4a)**. HCPT/S@CaP/HA also increased E-cadherin levels while reducing N-cadherin and MMP-9 expression, producing the strongest inhibitory effect on 4T1 migration and invasion among all treatment groups **(Figure 4b)**.

In the tumor microenvironment, CAF-derived CXCL12 activates the CXCL12/CXCR4 axis, promoting TNBC cell motility. HCPT/S@CaP/HA significantly decreased CXCL12 secretion from CAFs **(Figure 4c)** and exhibited the greatest inhibition of 4T1 migration and invasion in co-culture conditions **(Figure 4d)**. These findings indicate that HCPT/S@CaP/HA simultaneously reduces CXCR4 expression in tumor cells and suppresses CXCL12 production by CAFs, effectively disrupting the CXCL12/CXCR4 axis in both directions to enhance anti-metastatic activity.

Induction of dendritic cell maturation by HCPT/S@CaP/HA in vitro

Immunogenic cell death (ICD) generates key danger signals, including calreticulin (CRT) translocation to the cell surface, HMGB1 release, and ATP secretion [39]. ATP release occurs early, bridging the temporal gap

between CRT exposure and HMGB1 release (>12 h), together forming the triad of ICD that drives phagocytosis, recruitment, and activation of immune cells [40]. HCPT/S@CaP/HA treatment increased CRT exposure, HMGB1 release, and ATP secretion from 4T1 cells **(Figures 4e–4g)**, indicating effective ICD induction and release of tumor antigens.

CRT acts as an "eat-me" signal by binding CD97 on DCs, promoting antigen uptake [41], while HMGB1 engages TLR4 to activate DC signaling pathways [42]. Consequently, both signals enhance DC recognition and processing of tumor antigens, leading to upregulation of co-stimulatory molecules CD80 and CD86. HCPT/S@CaP/HA markedly increased CD80/CD86 expression on DCs **(Figures 4h–4i)**. Furthermore, co-culture with HCPT/S@CaP/HA-treated 4T1 cells significantly elevated IL-12 secretion by DCs **(Figure 4j)**, indicating robust functional maturation. These results demonstrate that HCPT/S@CaP/HA efficiently triggers ICD in 4T1 cells, promotes tumor antigen release, and enhances DC maturation in vitro [43].

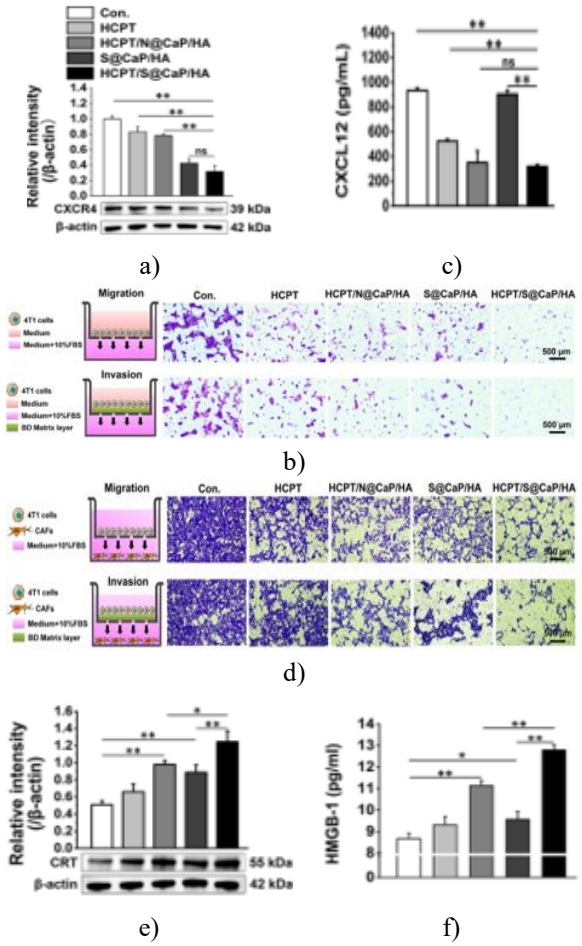

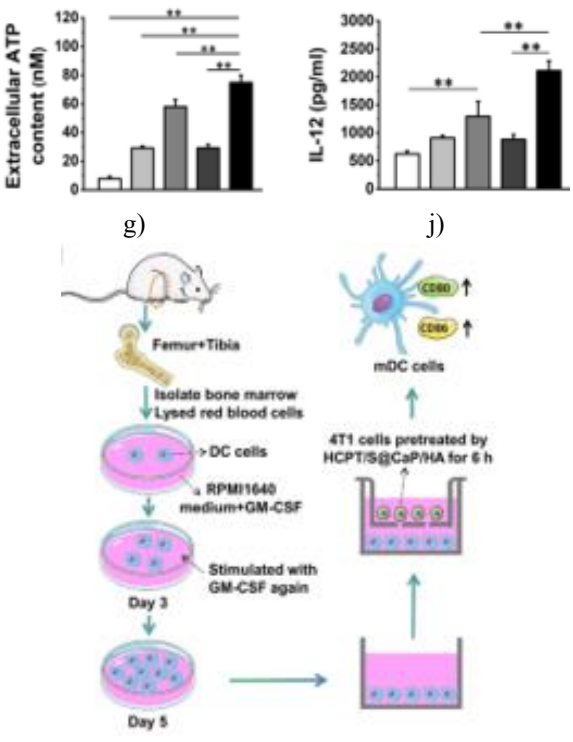

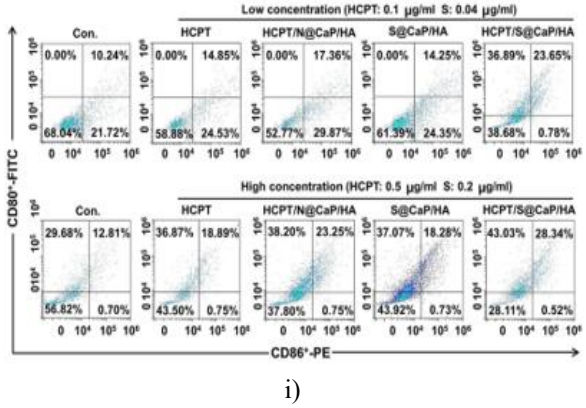

Figure 4. Effects of HCPT/S@CaP/HA on 4T1 Cell invasion and DC maturation in vitro. (a) CXCR4 expression in 4T1 cells following HCPT/S@CaP/HA treatment. (b) Migration and invasion of 4T1 cells without CAF co-culture. (c) CXCL12 secretion by CAFs. (d) Migration and invasion of 4T1 cells in the presence of CAFs. (e) CRT expression in 4T1 cells. (f) HMGB1 release from 4T1 cells. (g) ATP secretion by 4T1 cells. (h) Schematic of DC isolation and maturation after 6 h co-culture with HCPT/S@CaP/HA-pretreated 4T1 cells. (i) Flow cytometry analysis of $CD11c^{+}CD80^{+}CD86^{+}$ mature DCs. (j) IL-12 secretion by DCs in vitro. Data are expressed as mean ± SD, n = 3. *P < 0.05, **P < 0.01, ns: not significant. Statistical significance was

determined by one-way ANOVA with Dunnett's post-hoc test (a, c, g) or one-way ANOVA with Tukey's post-hoc test (e–f, j).

Biodistribution of HCPT/cy5-S@CaP/HA

Following 48 h stimulation with 4T1-conditioned medium (4T1-CM), human umbilical vein endothelial cells (HUVECs) displayed markedly increased CD44 expression, suggesting that HCPT/S@CaP/HA could recognize tumor-associated neovasculature, facilitating preferential accumulation within TNBC tissue. In vivo imaging revealed weak fluorescence in TNBC tissues but strong renal fluorescence after administration of free cy5-siCXCR4 plus HCPT, indicating rapid renal clearance. In contrast, HCPT/cy5-S@CaP/HA demonstrated significantly enhanced accumulation in orthotopic TNBC tissues, whereas HCPT/cy5-S@CaP/BSA showed reduced tumor localization, confirming HA-mediated active targeting via CD44. Co-localization imaging revealed overlap between green HCPT fluorescence and red α-SMA, indicating CAF targeting, while non-overlapping green fluorescence suggested direct delivery to 4T1 tumor cells.

HCPT/S@CaP/HA suppresses orthotopic TNBC growth by bidirectional CXCL12/CXCR4 blockade

Free HCPT exhibited limited inhibition of TNBC growth due to poor tumor accumulation, whereas S@CaP/HA suppressed tumor growth by silencing CXCR4 expression in TNBC cells. Co-delivery via HCPT/S@CaP/HA produced the strongest anti-tumor effect while mitigating body weight loss in treated mice **(Figures 5a–5c)**. Tumor weights in the HCPT/S@CaP/HA, HCPT/N@CaP/HA, and S@CaP/HA groups decreased by 72.45%, 35.05%, and 34.91%, respectively, compared to control, indicating a synergistic effect of combined HCPT and siCXCR4 delivery.

Histological examination of tumors from the HCPT/S@CaP/HA group revealed nuclear pyknosis, dispersed cancer cells, increased TUNEL-positive cells, and reduced Ki67 staining **(Figure 5d)**, demonstrating enhanced apoptosis and suppressed proliferation. During tumor progression, normal fibroblasts are recruited and transformed into CAFs by tumor-secreted cytokines [44]. CAF-derived CXCL12 engages CXCR4 on tumor cells, activating the CXCL12/CXCR4 axis to promote cell cycle progression and proliferation [45], while also upregulating anti-apoptotic proteins to prevent cell death [46]. HCPT/S@CaP/HA treatment markedly increased Bax and cleaved caspase-3 while decreasing Bcl-2 in orthotopic TNBC tissue.

Immunofluorescence and western blot analyses revealed high expression of CXCR4, α-SMA, FAP1, and CXCL12 in control TNBC tissue, which was significantly reduced following HCPT/S@CaP/HA treatment **(Figures 5e–5g)**. ELISA confirmed decreased CXCL12 levels in both tumor tissue and serum **(Figures 5h and 5i)**. Since the CXCL12/CXCR4 axis contributes to tumor angiogenesis [47], CD31 staining in HCPT/S@CaP/HA-treated tumors was markedly reduced. Collectively, these results demonstrate that HCPT/S@CaP/HA suppresses orthotopic TNBC growth by simultaneously inhibiting CAF-derived CXCL12 and silencing tumor CXCR4, achieving bidirectional blockade of the CXCL12/CXCR4 axis.

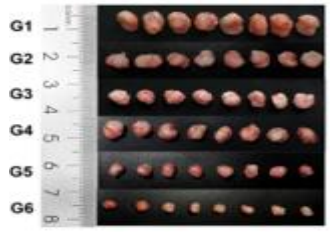

a)

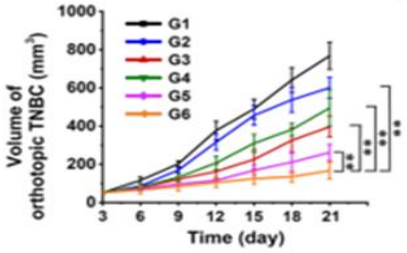

b)

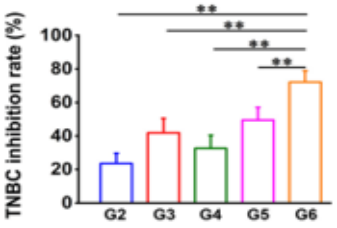

c)

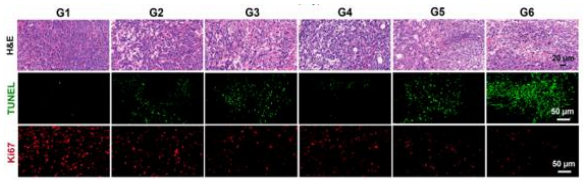

d)

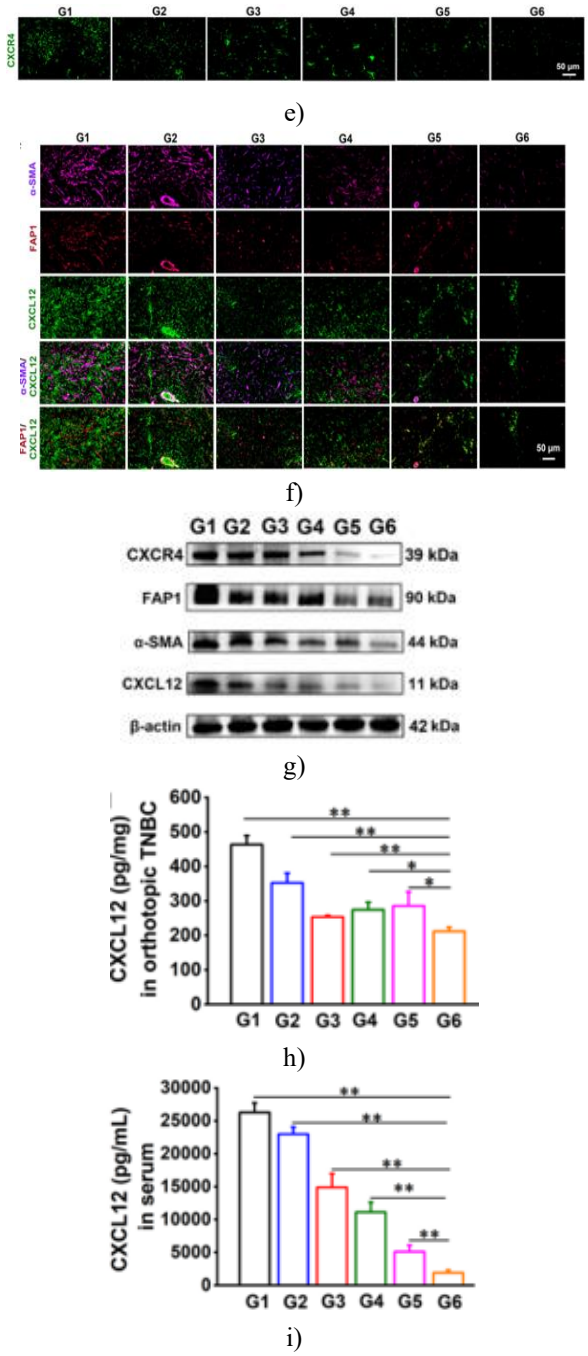

Figure 5. Inhibition of Orthotopic TNBC by HCPT/S@CaP/HA via CXCL12/CXCR4 Axis. (a) Representative images of orthotopic TNBC tissues. (b) Tumor volumes of orthotopic TNBC. (c) Tumor growth inhibition rate on day 21 post-implantation. (d) Histological analysis: H&E, TUNEL (green, apoptotic cells) and Ki67 (red, proliferating cells) staining. (e–f) Immunofluorescence of CXCR4, CXCL12, α-SMA, and FAP1 in TNBC tissue. (g) Western blot detection of CXCR4, CXCL12, α-SMA, and FAP1 in TNBC tissue. (h) CXCL12 levels in TNBC tissues. (i) CXCL12 levels in serum. Group designations: G1: model; G2: HCPT (3.9 mg/kg); G3: HCPT/N@CaP/HA (HCPT: 3.9 mg/kg, N: 1.0 mg/kg); G4: S@CaP/HA (S: 1.0 mg/kg); G5: HCPT/S@CaP/HA low dose (HCPT: 1.3 mg/kg, S: 0.3 mg/kg); G6: HCPT/S@CaP/HA high dose (HCPT: 3.9 mg/kg, S: 1.0 mg/kg). Data are mean ± SD, n = 3. *P < 0.05, **P < 0.01 (one-way ANOVA with Dunnett's post-hoc test).

HCPT/S@CaP/HA triggers anti-tumor immune responses in orthotopic TNBC models

Treatment with HCPT/N@CaP/HA and HCPT/S@CaP/HA significantly elevated CRT and HMGB1 expression in tumor tissues **(Figures 6a–6c)**, while HCPT/S@CaP/HA also markedly increased ATP levels within TNBC tissues **(Figure 6d)**. Furthermore, HCPT/N@CaP/HA enhanced the proportion of mature dendritic cells ($CD11c^+CD80^+CD86^+$) and cytotoxic T lymphocytes ($CD3^+CD8^+IFN\text{-}\gamma^+$) in the tumor microenvironment **(Figures 6e and 6f)**. Compared to control, the cytotoxic T cell fraction rose by 3.62%, 2.33%, and 0.85% in HCPT/S@CaP/HA, HCPT/N@CaP/HA, and S@CaP/HA groups, respectively, demonstrating synergistic enhancement through co-delivery of HCPT and siCXCR4.

HCPT/N@CaP/HA also promoted M1-type TAMs while reducing M2-TAMs in tumors **(Figures 6g–6i)**. The M1/M2 TAM ratios for HCPT/S@CaP/HA, HCPT/N@CaP/HA, S@CaP/HA, and control were 10.9, 5.0, 1.9, and 0.4, respectively, confirming synergistic remodeling of the TAM population. Additionally, HCPT/S@CaP/HA decreased neutrophil ($Ly6G^+$) and PMN-MDSC ($CD11b^+Gr\text{-}1^+$) infiltration. Pro-inflammatory cytokines TNF-α, IFN-γ, and IL-15 were upregulated, whereas immunosuppressive IL-6 and IL-10 were downregulated in tumor tissue and peripheral blood **(Figures 6j–6n)**. Specifically, TNF-α levels increased by 27.87, 12.8, and 5.91 pg/mg, and IFN-γ levels increased by 66.65, 39.29, and 23.12 pg/mg in HCPT/S@CaP/HA, HCPT/N@CaP/HA, and S@CaP/HA groups compared to control, highlighting the synergistic immunostimulatory effect of HCPT/S@CaP/HA.

These findings indicate that HCPT/S@CaP/HA induces immunogenic cell death of TNBC cells, enhances antigen presentation and processing by dendritic cells, and elicits TNBC-specific T cell responses. Normally, CAFs

produce high levels of CXCL12, generating a chemokine gradient that recruits immunosuppressive cells such as MDSCs and TAMs via CXCR4-mediated chemotaxis toward the tumor, suppressing anti-tumor immunity and promoting growth and metastasis [48, 49]. CXCL12 also polarizes TAMs to the M2 phenotype, which in turn stimulates CAF activation, creating an immunosuppressive feedback loop. By reducing CXCL12 secretion, HCPT/S@CaP/HA limits recruitment of immunosuppressive cells, increases the M1/M2 TAM ratio, and reverses the tumor's immunosuppressive environment, thereby enhancing cytotoxic T lymphocyte-mediated killing of TNBC cells.

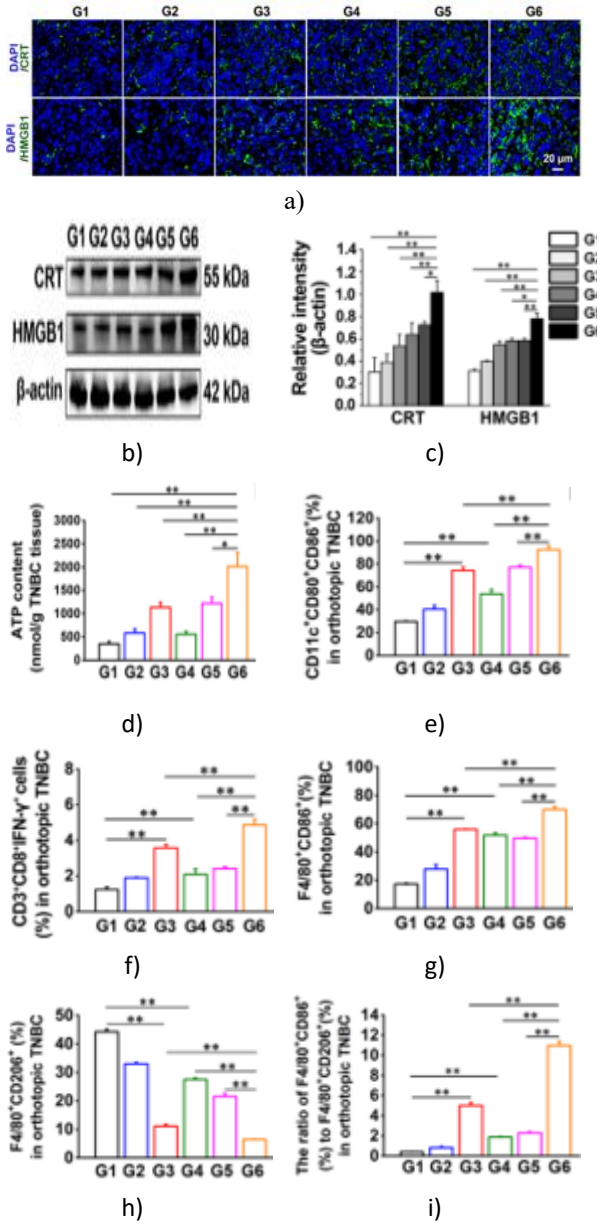

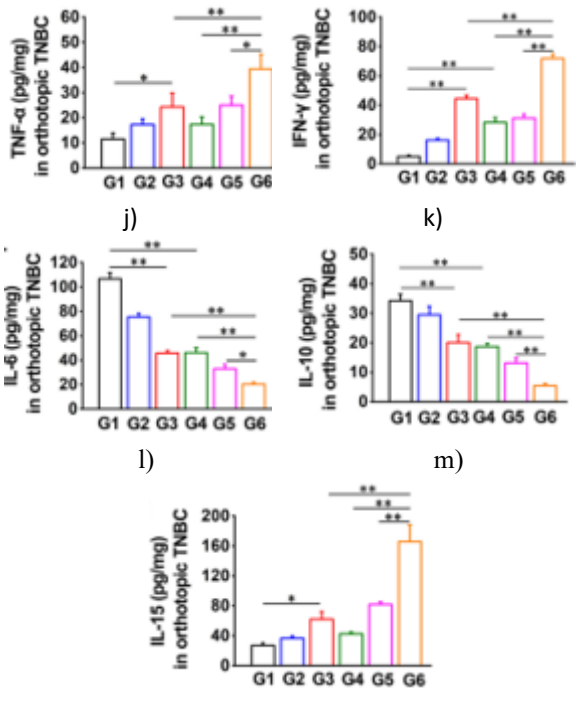

Figure 6. Anti-cancer immune responses in orthotopic TNBC mice following treatment with HCPT/S@CaP/HA. (a) Representative immunofluorescence images showing CRT and HMGB1 in orthotopic TNBC tissues. (b-c) Quantitative analysis of CRT and HMGB1 expression in these tissues. (d) Measurement of ATP content in orthotopic TNBC tissues. (e) Proportion of $CD11c^{+}CD80^{+}CD86^{+}$ cells. (f) Proportion of $CD3^{+}CD8^{+}IFN\text{-}\gamma^{+}$ T lymphocytes. (g) Proportion of $F4/80^{+}CD86^{+}$ TAMs. (h) Proportion of $F4/80^{+}CD206^{+}$ TAMs. (i) Ratio of M1-TAMs to M2-TAMs. (j-n) Levels of TNF-α, IFN-γ, IL-6, IL-10, and IL-15. Treatment groups were as follows: G1, model; G2, HCPT (3.9 mg/kg); G3, HCPT/N@CaP/HA (HCPT: 3.9 mg/kg, N: 1.0 mg/kg); G4, S@CaP/HA (S: 1.0 mg/kg); G5, HCPT/S@CaP/HA low dose (HCPT: 1.3 mg/kg, S: 0.3 mg/kg); G6, HCPT/S@CaP/HA high dose (HCPT: 3.9 mg/kg, S: 1.0 mg/kg). Data are expressed as mean ± SD, n = 3. *P < 0.05, **P < 0.01. Statistical analysis was performed using one-way ANOVA with Dunnett's test (C-D) or one-way ANOVA with Tukey's post-hoc test (e-n).

HCPT/S@CaP/HA inhibits distant TNBC growth through induction of immune memory

To further explore the immune memory effect induced by HCPT/S@CaP/HA, a cancer re-challenge model was established. The results demonstrated that HCPT/S@CaP/HA exhibited a significantly stronger inhibitory effect on distant TNBC growth compared with HCPT/N@CaP/HA and S@CaP/HA **(Figures 7a-7f)**. Moreover, distant TNBC tissues from HCPT/S@CaP/HA-treated mice showed extensive karyopyknosis and tumor cell lysis. The number of TUNEL-positive cells was markedly elevated, whereas Ki67-positive cells were significantly reduced **(Figure 7g)**, indicating that HCPT/S@CaP/HA effectively promoted apoptosis and suppressed proliferation in distant TNBC cells.

Firstly, the immune microenvironment of distant TNBC tissues was analyzed. Following HCPT/S@CaP/HA treatment, there was a notable increase in $CD44^+CD62L^+$ memory T lymphocytes, $CD3^+CD4^+IFN\text{-}\gamma^+$ type 1 helper T lymphocytes (Th1 cells), and $CD3^+CD8^+IFN\text{-}\gamma^+$ cytotoxic T lymphocytes, demonstrating enhanced infiltration of these immune cells into distant TNBC tissues. Compared to the control, cytotoxic T lymphocyte levels increased by 12.4%, 6.14%, and 1.12% in HCPT/S@CaP/HA, HCPT/N@CaP/HA, and S@CaP/HA groups, respectively, highlighting the synergistic effect of co-delivering HCPT and siCXCR4 via HCPT/S@CaP/HA.

Importantly, regulatory T lymphocytes ($CD4^+CD25^+FoxP3^+$) were significantly decreased, while the ratio of $F4/80^+CD86^+$ M1-TAMs to $F4/80^+CD206^+$ M2-TAMs was significantly elevated in distant TNBC tissues of HCPT/S@CaP/HA-treated mice. Specifically, the M1/M2-TAM ratios were 1.51, 0.83, 0.59, and 0.37 for HCPT/S@CaP/HA, HCPT/N@CaP/HA, S@CaP/HA, and control groups, respectively. These findings indicate that HCPT/S@CaP/HA synergistically promotes a shift toward a pro-inflammatory M1-TAM phenotype in distant TNBC tissues.

Overall, these data demonstrate that HCPT/S@CaP/HA effectively induces a potent immune memory response, enhances anti-tumor immunity, and reverses the immunosuppressive microenvironment in distant TNBC tissue.

Secondly, the generation of immune memory and modulation of the immune microenvironment in TNBC re-challenge mice were investigated. After the initial anti-cancer immune response subsides, most cytotoxic T lymphocytes are suppressed or eliminated, with only 5–10% surviving as long-lived memory T cells. Upon re-exposure to cancer antigens, these memory T cells are rapidly reactivated, proliferate, and differentiate into cytotoxic T lymphocytes capable of targeting tumor cells. Memory T lymphocytes also exhibit lymphatic homing capabilities [50]. In HCPT/S@CaP/HA-treated TNBC re-challenge mice, the proportion of $CD44^+CD62L^+$ memory T lymphocytes in the spleen was significantly elevated **(Figure 7h)**. Relative to the model group, memory T lymphocyte levels in the spleen increased by 6.53%, 3.18 percent, and 1.26 percent in the HCPT/S@CaP/HA, HCPT/N@CaP/HA, and S@CaP/HA groups, respectively, demonstrating that co-delivery of HCPT and siCXCR4 synergistically enhanced memory T cell formation in the spleen.

Type 1 helper T lymphocytes (Th1 cells) are crucial for activating $CD8^+$ T cells and promoting cellular immunity [51], and the spleen serves as a primary site for Th1 cell enrichment. Treatment with HCPT/S@CaP/HA significantly increased the proportions of $CD3^+CD4^+IFN\text{-}\gamma^+$ Th1 cells and $CD3^+CD8^+IFN\text{-}\gamma^+$ cytotoxic T lymphocytes in the spleens of TNBC re-challenge mice **(Figures 7i and 7j)**, indicating that HCPT/S@CaP/HA effectively induces immune memory. Upon TNBC cell reinvasion, memory T cells are reactivated and differentiate into cytotoxic T lymphocytes, assisted by Th1 cells, to eliminate distant TNBC cells.

Additionally, HCPT/S@CaP/HA markedly reduced $CD4^+CD25^+FoxP3^+$ regulatory T lymphocytes in the spleen **(Figure 7k)**. Concurrently, it significantly increased the proportion of $CD11c^+CD80^+CD86^+$ mature dendritic cells and elevated the ratio of $F4/80^+CD86^+$ M1-TAMs to $F4/80^+CD206^+$ M2-TAMs. Specifically, the M1/M2-TAM ratios in the spleens of TNBC re-challenge mice were 12.68, 3.37, 2.39, and 0.24 for HCPT/S@CaP/HA, HCPT/N@CaP/HA, S@CaP/HA, and control groups, respectively, showing that co-delivery of HCPT and siCXCR4 synergistically favors M1-TAM polarization. These results suggest that HCPT/S@CaP/HA reverses the immunosuppressive microenvironment in the spleen, facilitating memory T cell differentiation into cytotoxic T lymphocytes and enhancing the anti-TNBC immune response.

To assess whether these immune responses were tumor antigen-specific, a tumor antigen-specific T cell detection kit was employed to quantify effector tumor antigen-specific T cells (ETAST) in spleen tissues. After stimulation with 4T1 cell antigen, spleen immune cells

from TNBC re-challenge mice exhibited significant increases in $CD3^+IFN\text{-}\gamma^+$ T lymphocytes, $CD3^+CD4^+IFN\text{-}\gamma^+$ Th1 cells, and $CD3^+CD8^+IFN\text{-}\gamma^+$ cytotoxic T lymphocytes compared to unstimulated cells **(Figures 7l-7n)**, indicating that 4T1 antigens effectively triggered memory T cells and Th1 cells to differentiate into cytotoxic T lymphocytes.

Collectively, these findings demonstrate that HCPT/S@CaP/HA effectively prevents TNBC recurrence by inducing immune memory, activating tumor-specific immune responses, and reversing the immunosuppressive microenvironment in distant TNBC tissues.

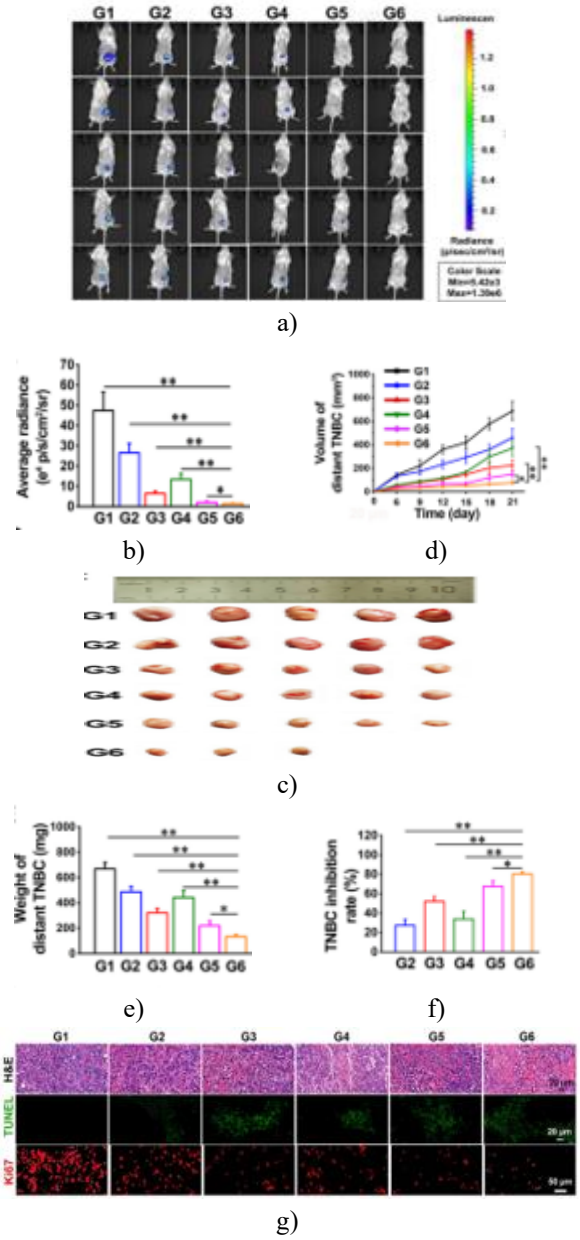

Figure 7. Inhibitory effects of HCPT/S@CaP/HA on distant TNBC growth and its underlying mechanisms. (a-b) Bioluminescence imaging and quantification of fluorescence intensity in distant TNBC tissue (n = 5). (c) Representative images of distant TNBC tissue. (d) Tumor volume (n = 5). (e) Tumor weight (n = 5). (f) Tumor growth inhibition rate (n = 5). (g) H&E, TUNEL, and Ki67 staining of distant TNBC tissue, with green indicating TUNEL-positive cells and red indicating Ki67-positive cells. (h-k) Immune cell proportions in spleen tissue, including $CD44^+CD62L^+$ memory T cells, $CD3^+CD4^+IFN\text{-}\gamma^+$ Th1 cells, $CD3^+CD8^+IFN\text{-}\gamma^+$ cytotoxic T cells, and $CD4^+CD25^+FoxP3^+$ regulatory T cells. (l-n) Quantification of $CD3^+IFN\text{-}\gamma^+$, $CD3^+CD4^+IFN\text{-}\gamma^+$, and $CD3^+CD8^+IFN\text{-}\gamma^+$ T cells in spleen following stimulation with 4T1 cell-derived antigens. Treatment groups were: G1, model; G2, HCPT (3.9 mg/kg); G3, HCPT/N@CaP/HA (HCPT: 3.9 mg/kg, N: 1.0 mg/kg); G4, S@CaP/HA (S: 1.0 mg/kg); G5, HCPT/S@CaP/HA low dose (HCPT: 1.3 mg/kg, S: 0.3 mg/kg); G6, HCPT/S@CaP/HA high dose (HCPT: 3.9 mg/kg, S: 1.0 mg/kg). Data are expressed as mean ± SD, n = 3. *P < 0.05, **P < 0.01.

Statistical analysis was performed via one-way ANOVA with Dunnett's test (b, d-f) or Tukey's post-hoc test (h-n).

HCPT/S@CaP/HA suppresses spontaneous lung metastasis of orthotopic TNBC via adaptive immunity

To assess anti-metastatic efficacy, luciferase-labeled 4T1 cells were implanted into the fourth pair of mammary pads of female BALB/c mice. Mice treated with HCPT/S@CaP/HA exhibited the lowest metastatic fluorescence in lungs, the fewest metastatic nodules, and the lightest lung weights **(Figures 8a-8d)**. Histological examination showed a marked reduction in TNBC metastatic foci (black arrow; pan-CK positive cells) in the lungs of HCPT/S@CaP/HA-treated mice **(Figure 8e)**, confirming effective inhibition of spontaneous lung metastasis.

Immunofluorescence analysis revealed that α-SMA, FAP1, and CXCL12 expression in lung tissue was significantly decreased following HCPT/S@CaP/HA treatment **(Figure 8f)**, indicating that as an in situ cancer nanovaccine, HCPT/S@CaP/HA suppressed CAF formation and reduced CXCL12 secretion. Concurrently, HCPT/S@CaP/HA increased $CD8^+$ T cell and M1 macrophage infiltration while reducing MDSCs and M2 macrophages in the lung **(Figure 9a)**, demonstrating enhanced anti-tumor immune cell recruitment and decreased immunosuppressive cell infiltration.

The sentinel lymph node (SLN) adjacent to the fourth mammary pad was evaluated. Both SLN size and weight were markedly reduced in HCPT/N@CaP/HA and S@CaP/HA groups. TNBC cells metastasize from SLN to ipsilateral axillary lymph nodes (IALN), causing enlargement and inflammation. HCPT/S@CaP/HA treatment significantly reduced IALN size and weight. The number of pan-CK-positive TNBC cells in SLN and IALN was greatly diminished in HCPT/S@CaP/HA-treated mice compared with the model group **(Figure 9b)**, confirming inhibition of lymphatic metastasis.

cDC1s, a dendritic cell subset specialized in antigen cross-presentation, migrate to SLN to activate $CD8^+$ T cells and initiate tumor-specific immune responses. Immunofluorescence demonstrated increased infiltration of $CD11c^+CD103^+$ DCs (cDC1s) in SLN following HCPT/S@CaP/HA treatment, supporting enhanced antigen presentation and subsequent TNBC clearance in metastatic lymph nodes **(Figure 9c)**. Furthermore, HCPT/S@CaP/HA elevated cytotoxic T lymphocytes and the M1/M2 macrophage ratio in the spleen **(Figures 9d-9g)**, indicating systemic activation of adaptive immunity in spontaneous lung metastatic TNBC mice.

HCPT/S@CaP/HA also modulated EMT markers in orthotopic TNBC tissue, increasing E-cadherin while reducing N-cadherin and MMP-9 expression, thereby limiting EMT-mediated invasion and extracellular matrix degradation.

Normal lung fibroblasts are typically transformed into CAFs by tumor-derived secreted factors (TDSFs) [52, 53]. CAFs in both lung and orthotopic TNBC tissues secrete CXCL12, activating the CXCL12/CXCR4 axis and promoting lung metastasis through three main mechanisms: (1) TNBC cells acquire enhanced adhesion, migration, and invasion via EMT induction [54]; CXCL12 also disrupts endothelial tight junctions, increasing vascular permeability [55] to facilitate intravasation; (2) disseminated TNBC cells evade immune surveillance due to systemic immunosuppression [56, 57]; (3) MDSCs and monocytes are recruited to lung tissue, differentiating into M2 macrophages that suppress cytotoxic T cell activity, creating a pre-metastatic niche favorable for TNBC colonization [58–60].

Collectively, these results indicate that HCPT/S@CaP/HA effectively blocks spontaneous lung metastasis of orthotopic TNBC by directly killing tumor cells, inhibiting EMT, enhancing antigen presentation, activating systemic adaptive immunity, remodeling the pulmonary immune microenvironment, and disrupting the CXCL12/CXCR4-mediated lung tropism of TNBC cells.

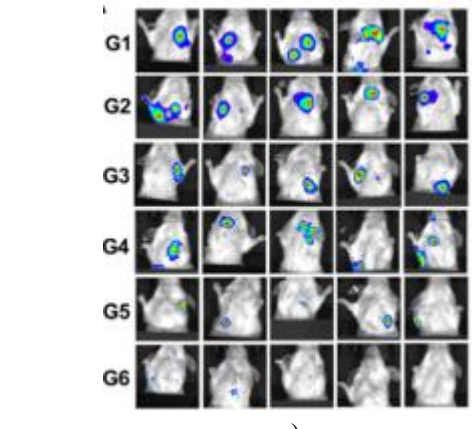

a)

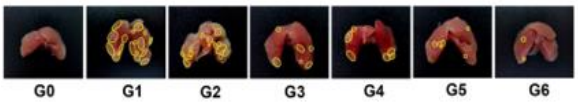

b)

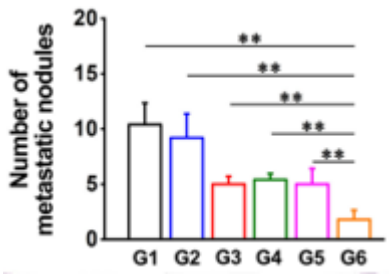

c)

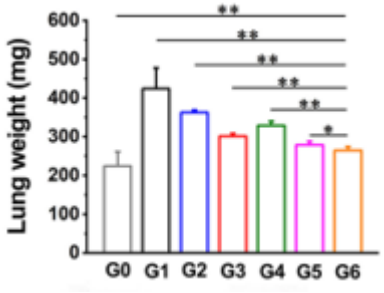

d)

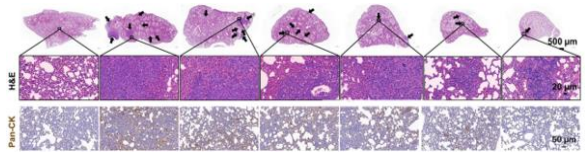

e)

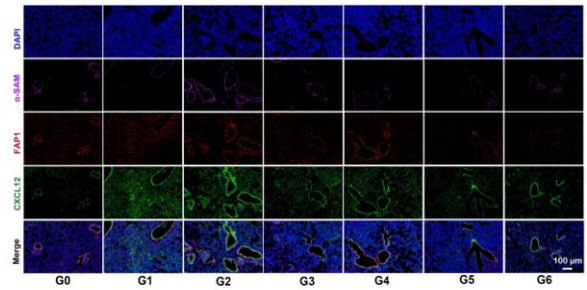

f)

Figure 8. Antimetastatic effects of HCPT/S@CaP/HA nanoparticles in a mouse model of orthotopic triple-negative breast cancer (TNBC) with spontaneous lung metastasis. (a) In vivo bioluminescence imaging showing lung metastatic signals in orthotopic TNBC-bearing mice across treatment groups. (b) Representative images of excised lungs highlighting metastatic nodules (indicated by yellow circles). (c) Quantification of metastatic lung nodules per mouse. (d) Lung weight measurements as an indicator of metastatic burden. (e) Histological analysis of lung sections using hematoxylin and eosin (H&E) staining and immunohistochemical staining for pan-cytokeratin (pan-CK), a marker of metastatic TNBC cells. (f) Immunofluorescence staining for α-smooth muscle actin (α-SMA), fibroblast activation protein (FAP), and CXCL12 in lung tissue, reflecting remodeling of the premetastatic niche.

Treatment groups:
G0: Healthy control mice.
G1: Untreated TNBC model.
G2: Free hydroxycamptothecin (HCPT) at 3.9 mg/kg.
G3: HCPT combined with control siRNA (N) encapsulated in CaP/HA nanoparticles (HCPT: 3.9 mg/kg; N: 1.0 mg/kg).
G4: siCXCR4 (S) encapsulated in CaP/HA nanoparticles (S: 1.0 mg/kg).
G5: Low-dose HCPT/S@CaP/HA (HCPT: 1.3 mg/kg; S: 0.3 mg/kg).
G6: High-dose HCPT/S@CaP/HA (HCPT: 3.9 mg/kg; S: 1.0 mg/kg).
Results are expressed as mean ± standard deviation (n = 5 per group). Statistical differences: *P < 0.05, **P < 0.01 (one-way ANOVA followed by Dunnett's post-hoc test).

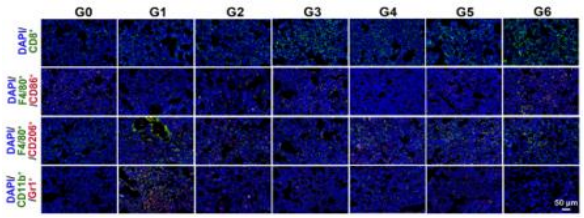

a)

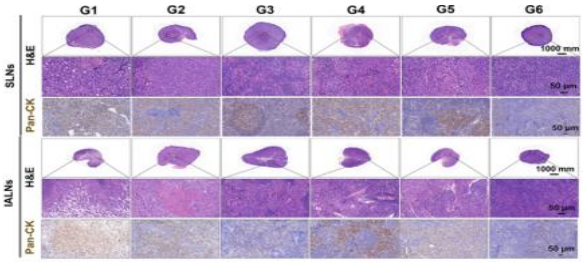

b)

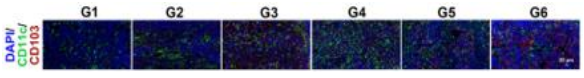

c)

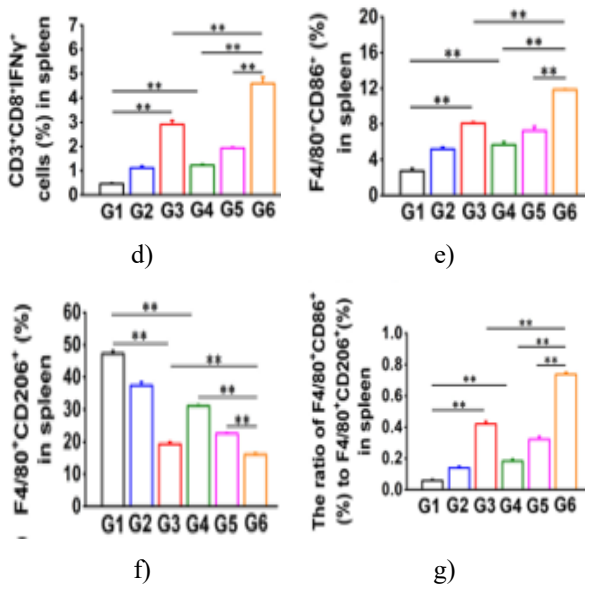

Figure 9. Immunomodulatory effects of HCPT/S@CaP/HA on the immune microenvironment in lung tissue and tumor-draining lymph nodes in a mouse model of spontaneous lung metastasis from orthotopic triple-negative breast cancer (TNBC). (a) Representative immunofluorescence images of lung tissue showing infiltration of $CD8^+$ T lymphocytes, M1 macrophages ($F4/80^+CD86^+$ cells), M2 macrophages ($F4/80^+CD206^+$ cells), and myeloid-derived suppressor cells (MDSCs; $CD11b^+Gr1^+$ cells). (b) Hematoxylin and eosin (H&E) staining and immunohistochemical staining for pan-cytokeratin (pan-CK, a marker of metastatic TNBC cells) in sentinel lymph nodes (SLNs) and inguinal/axillary lymph nodes (IALNs). (c) Representative immunofluorescence images of conventional type 1 dendritic cells (cDC1s; $CD11c^+CD103^+$ cells) in SLNs. (d) Flow cytometry quantification of cytotoxic T lymphocytes ($CD3^+CD8^+IFN\text{-}\gamma^+$ cells) in spleen tissue. (e) Proportion of M1 macrophages ($F4/80^+CD86^+$) in spleen tissue. (f) Proportion of M2 macrophages ($F4/80^+CD206^+$) in spleen tissue. (g) Ratio of M1 to M2 macrophages in spleen tissue.

Treatment groups:
G0: Healthy control mice.
G1: Untreated TNBC model.
G2: Free hydroxycamptothecin (HCPT) at 3.9 mg/kg.
G3: HCPT combined with control siRNA (N) in CaP/HA nanoparticles (HCPT: 3.9 mg/kg; N: 1.0 mg/kg).
G4: siCXCR4 (S) in CaP/HA nanoparticles (S: 1.0 mg/kg).
G5: Low-dose HCPT/S@CaP/HA (HCPT: 1.3 mg/kg; S: 0.3 mg/kg).
G6: High-dose HCPT/S@CaP/HA (HCPT: 3.9 mg/kg; S: 1.0 mg/kg).
Data are shown as mean ± standard deviation (n = 3). **P < 0.01 (one-way ANOVA with Tukey's post-hoc test for panels D–G).

The results indicate that high-dose HCPT/S@CaP/HA treatment markedly enhanced antitumor immunity by increasing $CD8^+$ T cell infiltration and M1 macrophages while reducing immunosuppressive M2 macrophages and MDSCs in lung tissue. It also promoted cDC1 accumulation in lymph nodes and shifted splenic macrophage polarization toward an M1 phenotype, elevating the M1/M2 ratio and cytotoxic T cell proportions.

In vivo safety evaluation

Free HCPT significantly reduced white blood cell (WBC) and platelet (PLT) counts, indicating hematological toxicity. In contrast, HCPT/S@CaP/HA treatment maintained normal WBC and PLT levels. Serum biomarkers of cardiac (creatine kinase, CK; lactic dehydrogenase, LDH), liver (alanine aminotransferase, ALT; aspartate aminotransferase, AST), and kidney (blood urea nitrogen, BUN; creatinine, CREA; uric acid, UA) function remained within normal ranges in the HCPT/S@CaP/HA group. Histopathological examination revealed no evident damage to major organs (brain, heart, liver, spleen, lung, kidney) following HCPT/S@CaP/HA administration, demonstrating improved safety profile compared to free HCPT at therapeutic doses.

Conclusion

This study successfully developed an in situ cancer nanovaccine, HCPT/S@CaP/HA, which actively targets TNBC cells and cancer-associated fibroblasts (CAFs) via hyaluronic acid (HA)-mediated recognition of overexpressed CD44 on tumor neovasculature, TNBC cells, and CAFs. HCPT triggered immunogenic cell death (ICD) in orthotopic TNBC, promoting dendritic cell (DC) maturation and T cell-mediated antitumor immunity. Concurrent delivery of siCXCR4 downregulated CXCL12 secretion from CAFs and CXCR4 expression in tumor cells, bidirectionally

disrupting the CXCL12/CXCR4 axis. This synergy reversed immunosuppression in primary tumors by limiting neutrophil recruitment and favoring M1 over M2 tumor-associated macrophage polarization, thereby inhibiting orthotopic TNBC growth.

Additionally, HCPT/S@CaP/HA activated splenic memory T cells, reinvigorating TNBC-specific systemic immunity and preventing tumor recurrence. In the spontaneous lung metastasis model, the nanovaccine countered CXCL12/CXCR4-driven immunosuppression in both primary and lung tissues, enhanced antigen presentation, and bolstered adaptive immunity. This led to reduced M2 macrophages and MDSCs, increased $CD8^+$ T cell infiltration in lungs, disruption of the premetastatic niche, and significant inhibition of lung metastasis.

Overall, co-delivery of HCPT and siCXCR4 via HCPT/S@CaP/HA effectively induced ICD, matured DCs, and synergistically activated local and systemic antitumor immune responses, ultimately suppressing growth, recurrence, and lung metastasis of TNBC.

This work offers a novel immunotherapeutic strategy for TNBC but has limitations: (1) Efficacy against liver, brain, or bone metastases remains untested; (2) Long-term toxicity requires evaluation in larger animals (e.g., dogs) at higher doses; (3) Validation in other solid tumors (e.g., gastric, liver, colorectal cancer) is needed to broaden clinical applicability.

Acknowledgments: None

Conflict of Interest: None

Financial Support: None

Ethics Statement: None

References

1. Peng Z, Zhao T, Gao P, et al. Tumor-derived extracellular vesicles enable tumor tropism chemo-genetherapy for local immune activation in triple-negative breast cancer. ACS Nano. 2024;18(45):30943–56.
2. Jiang Y, Ma D, Suo C, et al. Genomic and transcriptomic landscape of triple-negative breast cancers: subtypes and treatment strategies. Cancer Cell. 2019;35(3):428–40.
3. Sharma P, Otto M. Multifunctional nanocomposites modulating the tumor microenvironment for enhanced cancer immunotherapy. Bioact Mater. 2024;31:440–62.
4. Chen M, Bie L, Ying J. Cancer cell-intrinsic PD-1: its role in malignant progression and immunotherapy. Biomed Pharmacother. 2023;167:115514.
5. Andrews LP, Yano H, Vignali DAA. Inhibitory receptors and ligands beyond PD-1, PD-L1 and ctla-4: breakthroughs or backups. Nat Immunol. 2019;20(11):1425–34.
6. Guo B, Yang F, Zhang L, et al. Cuproptosis induced by ROS responsive nanoparticles with elesclomol and copper combined with alphapd-l1 for enhanced cancer immunotherapy. Adv Mater. 2023;35(22):e2212267.
7. Malla RR, Vasudevaraju P, Vempati RK, et al. Regulatory t cells: their role in triple-negative breast cancer progression and metastasis. Cancer. 2022;128(6):1171–83.
8. Liu Y, Hu Y, Xue J, et al. Advances in immunotherapy for triple-negative breast cancer. Mol Cancer. 2023;22(1):145.
9. Yu Z, Wang D, Qi Y, et al. Autologous-cancer-cryoablation-mediated nanovaccine augments systematic immunotherapy. Mater Horiz. 2023;10(5):1661–77.
10. An X, Chen Z, Luo Y, et al. Light-activated in situ vaccine with enhanced cytotoxic t lymphocyte infiltration and function for potent cancer immunotherapy. Adv Sci (Weinh). 2024;11(33):e2403158.
11. Gong N, Alameh M, El-Mayta R, et al. Enhancing in situ cancer vaccines using delivery technologies. Nat Rev Drug Discov. 2024;23(8):607–25.
12. Li R, Chen Z, Li J, et al. Nano-drug delivery systems for t cell-based immunotherapy. Nano Today. 2022;46:16. Article Google Scholar
13. Mousavi A. CXCL12/CXCR4 signal transduction in diseases and its molecular approaches in targeted-therapy. Immunol Lett. 2020;217:91–115.
14. Xie Y, Hang Y, Wang Y, et al. Stromal modulation and treatment of metastatic pancreatic cancer with local intraperitoneal triple mirna/sirna nanotherapy. ACS Nano. 2020;14(1):255–71.
15. Alghamri MS, Banerjee K, Mujeeb AA, et al. Systemic delivery of an adjuvant CXCR4-CXCL12 signaling inhibitor encapsulated in synthetic protein

nanoparticles for glioma immunotherapy. ACS Nano. 2022;16(6):8729–50.
16. Gonzalez H, Hagerling C, Werb Z. Roles of the immune system in cancer: from tumor initiation to metastatic progression. Genes Dev. 2018;32(19–20):1267–84.
17. Tsoumakidou M. The advent of immune stimulating CAFs in cancer. Nat Rev Cancer. 2023;23(4):258–69.
18. Shen L, Li J, Liu Q, et al. Local Blockade of Interleukin 10 and C-X-C motif chemokine ligand 12 with nano-delivery promotes antitumor response in murine cancers. ACS Nano. 2018;12(10):9830–41.
19. Dong J, Zhu C, Zhang F, et al. Attractive/adhesion force dual-regulatory nanogels capable of cxcr4 antagonism and autophagy Inhibition for the treatment of metastatic breast cancer. J Control Release. 2022;341:892–903.
20. Scala S. Molecular pathways: targeting the CXCR4-CXCL12 axis–untapped potential in the tumor microenvironment. Clin Cancer Res. 2015;21(19):4278–85.
21. Zhou M, Luo C, Zhou Z, et al. Improving anti-PD-L1 therapy in triple negative breast cancer by polymer-enhanced Immunogenic cell death and CXCR4 Blockade. J Control Release. 2021;334:248–62.
22. Zhou W, Guo S, Liu M, et al. Targeting CXCL12/CXCR4 axis in tumor immunotherapy. Curr Med Chem. 2019;26(17):3026–41.
23. Dong J, Zhu C, Huang Y, et al. Reversing the PAI-1-induced fibrotic immune exclusion of solid tumor by multivalent CXCR4 antagonistic nano-permeator. Acta Pharm Sin B. 2023;13(7):3106–20.
24. Zhou M, Liu C, Li B, et al. Cell surface patching via CXCR4-targeted nanothreads for cancer metastasis Inhibition. Nat Commun. 2024;15(1):2763.
25. Zhang J, Wang B, Wang H, et al. Reversibly double locked hydroxycamptothecin prodrug nanoparticles for targeted chemotherapy of lung cancer. Acta Biomater. 2023;166:593–603.
26. Lei L, Yan J, Xin K, et al. Engineered bacteriophage-based in situ vaccine remodels a tumor microenvironment and elicits potent antitumor immunity. ACS Nano. 2024;18(19):12194–209.
27. Zeng S, Ou H, Gao Z, et al. Hcpt-peptide prodrug with tumor microenvironment -responsive morphology transformable characteristic for boosted bladder tumor chemotherapy. J Control Release. 2021;330:715–25.
28. Chen Q, Huang J, Ye Y, et al. Delivery of hydroxycamptothecin via sonoporation: an effective therapy for liver fibrosis. J Control Release. 2023;358:319–32.
29. Paunovska K, Loughrey D, Dahlman JE. Drug delivery systems for RNA therapeutics. Nat Rev Genet. 2022;23(5):265–80.
30. Lu Z, Shen J, Yang J, et al. Nucleic acid drug vectors for diagnosis and treatment of brain diseases. Signal Transduct Target Ther. 2023;8(1):39.
31. Hu B, Zhong L, Weng Y, et al. Therapeutic sirna: state of the Art. Signal Transduct Target Ther. 2020;5(1):101.
32. Tang Q, Khvorova A. RNAi-based drug design: considerations and future directions. Nat Rev Drug Discov. 2024;23(5):341–64.
33. Brogna MR, Varone V, Delsesto M, et al. The role of CAFs in therapeutic resistance in triple negative breast cancer: an emerging challenge. Front Mol Biosci. 2025;12:1568865.
34. Sebastian A, Hum NR, Martin KA, et al. Single-cell transcriptomic analysis of tumor-derived fibroblasts and normal tissue-resident fibroblasts reveals fibroblast heterogeneity in breast cancer. Cancers (Basel). 2020;12(5):22. Article Google Scholar
35. Sun E, Choi J, Park M, et al. Fgfr4 promotes Caf activation through the cxcl10-cxcr3 axis in colon cancer. Cell Death Dis. 2025;16(1):424.
36. Zou J, Jiang C, Hu Q, et al. Tumor microenvironment-responsive engineered hybrid nanomedicine for photodynamic-immunotherapy via multi-pronged amplification of reactive oxygen species. Nat Commun. 2025;16(1):424.
37. Chao Y, Lee Y, Tseng C, et al. Improved cap nanoparticles for nucleic acid and protein delivery to neural primary cultures and stem cells. ACS Nano. 2024;18(6):4822–39.
38. Wu H, Lin J, Liu Y, et al. Luteolin suppresses androgen receptor-positive triple-negative breast cancer cell proliferation and metastasis by epigenetic regulation of MMP9 expression via the AKT/MTOR signaling pathway. Phytomedicine. 2021;81:153437.
39. Peng J, Li S, Ti H. Sensitize tumor immunotherapy: Immunogenic cell death inducing nanosystems. Int J Nanomed. 2024;19:5895–930.

40. Galluzzi L, Kepp O, Hett E, et al. Immunogenic cell death in cancer: concept and therapeutic implications. J Transl Med. 2023;21(1):162.
41. Jiang X, Wu L, Zhang M, et al. Biomembrane nanostructures: multifunctional platform to enhance tumor chemoimmunotherapy via effective drug delivery. J Control Release. 2023;361:510–33.
42. Huang J, Duan F, Xie C, et al. Microbes mediated Immunogenic cell death in cancer immunotherapy. Immunol Rev. 2024;321(1):128–42.
43. Shen M, Wang Y, Bing T, et al. Alendronate triggered dual-cascade targeting prodrug nanoparticles for enhanced tumor penetration and Sting activation of osteosarcoma. Adv Funct Mater. 2023;33(49):15.
44. Chen X, Song E. Turning foes to friends: targeting cancer-associated fibroblasts. Nat Rev Drug Discov. 2019;18(2):99–115.
45. Hang Y, Tang S, Tang W, et al. Polycation fluorination improves intraperitoneal Sirna delivery in metastatic pancreatic cancer. J Control Release. 2021;333:139–50.
46. Shi Y, Riese DJN, Shen J. The role of the cxcl12/cxcr4/cxcr7 chemokine axis in cancer. Front Pharmacol. 2020;11:574667.
47. Yang Y, Li J, Lei W, et al. CXCL12-CXCR4/CXR7 axis in cancer: from mechanisms to clinical applications. Int J Biol Sci. 2023;19(11):3341–59.
48. Zhang S, Jiang H, Zhao C, et al. CXCL12-targeting Sirna nanoparticles alleviate immunosuppression and inhibit tumor progression in esophageal squamous cell carcinoma. J Nanobiotechnol. 2025;23(1):519.
49. Bai H, Zhu X, Gao L, et al. Erg mediates the differentiation of hepatic progenitor cells towards immunosuppressive PDGFRα+ cancer-associated fibroblasts during hepatocarcinogenesis. Cell Death Dis. 2025;16(1):26.
50. Corrado M, Pearce EL. Targeting memory t cell metabolism to improve immunity. J Clin Invest. 2022;132(1):e148546.
51. Sun L, Su Y, Jiao A, et al. T cells in health and disease. Signal Transduct Target Ther. 2023;8(1):235.
52. Liu Y, Cao X. Characteristics and significance of the pre-metastatic niche. Cancer Cell. 2016;30(5):668–81.
53. Wu F, Yang J, Liu J, et al. Signaling pathways in cancer-associated fibroblasts and targeted therapy for cancer. Signal Transduct Target Ther. 2021;6(1):218.
54. Kawakita E, Yang F, Kumagai A, et al. Metformin mitigates DPP-4 inhibitor-induced breast cancer metastasis via suppression of Mtor signaling. Mol Cancer Res. 2021;19(1):61–73.
55. Ahirwar DK, Nasser MW, Ouseph MM, et al. Fibroblast-derived cxcl12 promotes breast cancer metastasis by facilitating tumor cell intravasation. Oncogene. 2018;37(32):4428–42.
56. Altorki NK, Markowitz GJ, Gao D, et al. The lung microenvironment: an important regulator of tumour growth and metastasis. Nat Rev Cancer. 2019;19(1):9–31.
57. Wu Q, You L, Nepovimova E, et al. Hypoxia-inducible factors: master regulators of hypoxic tumor immune escape. J Hematol Oncol. 2022;15(1):77.
58. Mcginnis CS, Miao Z, Superville D, et al. The Temporal progression of lung immune remodeling during breast cancer metastasis. Cancer Cell. 2024;42(6):1018–31.
59. Xu X, Wang Q, Qian X, et al. Spatial-drug-laden protease-activatable M1 macrophage system targets lung metastasis and potentiates antitumor immunity. ACS Nano. 2023;17(6):5354–72.
60. Casanova-Acebes M, Dalla E, Leader AM, et al. Tissue-resident macrophages provide a pro-tumorigenic niche to early Nsclc cells. Nature. 2021;595(7868):578–84.